Available online at www.sciencedirect.com
ScienceDirect
Optical Materials 29 (2007) 1693–1699
OPTICAL Materials
www.elsevier.com/locate/optmat

Partition, luminescence and energy transfer of Er^{3+}/Yb^{3+} ions in oxyfluoride glass ceramic containing CaF_2 nano-crystals

Daqin Chen, Yuansheng Wang *, En Ma, Yunlong Yu, Feng Liu

State Key Laboratory of Structural Chemistry, Fujian Institute of Research on the Structure of Matter, Chinese Academy of Sciences, Fuzhou, Fujian 350002, China

Received 12 June 2006; received in revised form 21 September 2006; accepted 21 September 2006
Available online 1 November 2006

Abstract

A complete spectroscopic investigation of energy transfer processes in oxyfluoride glass ceramics containing CaF_2 nano-crystals doped with various amounts of Er^{3+} and Yb^{3+} was reported. An enhancement of the 1.53 μm emission and infrared to visible up-conversion fluorescence was confirmed experimentally due to efficient non-radiative energy transfer from Yb^{3+} to Er^{3+} ions concentrated in CaF_2 nano-crystals. The efficiency of Yb^{3+} to Er^{3+} energy transfer in excess of 85% was obtained for 0.5 mol% Er^{3+}/2.0 mol% Yb^{3+} co-doped glass ceramic. Using rate equation formulism, the coefficient of Yb^{3+} to Er^{3+} energy transfer was determined to be about 3.5 times higher than that of Er^{3+} to Yb^{3+} energy back transfer, which is sufficient to provide high $^4I_{11/2}$ population of Er^{3+} to improve the fluorescence of the co-doped glass ceramics.

PACS: 81.05.Y; 42.70

Keywords: Oxyfluoride glass ceramics; CaF_2 nano-crystals; Energy transfer; Iuminescence; Up-conversion

1. Introduction

In order to improve the fluorescence properties of erbium ions, it is well known that the fluoride environment is preferred over the oxide one mainly to avoid non-radiative transitions [1]. The solubility of the rare earth is also larger in the fluoride medium than in the oxide [2]. Among fluorides, CaF_2 is a promising candidate of desired host materials for its high solubility of both sensitizer and activator rare earth ions and highly transparent from 0.13 to 9.5 μm [3]. However, the synthesis of fluoride crystals is complicated, and the stability and fiberizability as practical materials still remain problematic. Thus, a good solution would be Er^{3+}-doped oxyfluoride glass ceramic composite, i.e., fluoride crystallites embedded among an oxide glassy matrix with high chemical and mechanical stabilities [4–7]. The advantages of this kind of materials are that the rare earth ions would be incorporated selectively into the fluoride crystalline phase after crystallization, and these materials could remain good transparency due to much smaller size of precipitated crystals than the wavelength of visible light [8].

Er^{3+}-doped glass ceramics containing CaF_2 nano-crystals has been recently reported and demonstrated having potential application as the red up-conversion material and Er^{3+}-doped fiber amplifier [9,10]. In order to improve the emission of Er^{3+}, the sensitization of this nano-composite with Yb^{3+} ions may be a good choice because of the efficient energy transfer from Yb^{3+} to Er^{3+} ions. In this work, we studied the partition of rare earth ions, the infrared fluorescence, the up-conversion fluorescence and the energy transfer and back transfer processes in Er^{3+}/Yb^{3+} co-doped glass ceramics containing CaF_2 nano-crystals.

* Corresponding author. Tel./fax: +86 591 8370 5402.
E-mail address: yswang@fjirsm.ac.cn (Y. Wang).

0925-3467/$ - see front matter © 2006 Elsevier B.V. All rights reserved.
doi:10.1016/j.optmat.2006.09.002

2. Experimental

The Er^{3+}/Yb^{3+} co-doped precursor glasses were prepared with the following composition (in mol%): $45SiO_2$–$25Al_2O_3$–5CaO–10NaF–$15CaF_2$–$0.5ErF_3$–$xYbF_3$ ($x = 0.1$, 0.5, 1.0 and 2.0, respectively). In addition, in order to investigate the energy transfer efficiency, Yb^{3+} single-doped (the concentration was 0.1, 0.5, 1.0 and 2.0 mol%, respectively) precursor glasses of the same matrix were also fabricated. For each batch, about 20 g of starting materials were fully mixed and melted in a covered platinum crucible in air atmosphere at 1350 °C for 1.5 h, and then cast into a brass mold followed by annealing to relinquish the inner stress. The precursor glasses thus obtained were then heated and hold for 2 h at 650 °C to induce crystallization. To characterize the crystallization phase, X-ray diffraction (XRD, DMAX2500 RIGAKU) analysis and transmission electron microscopy (TEM, JEM-2010, equipped with the energy dispersive X-ray spectroscopy system) observation were carried out. The absorption spectra were recorded on a spectrophotometer (Lambda900, Perkin–Elmer) with a spectral range from 200 to 2000 nm and a resolution of 1.0 nm. By using an InP/InGaAs photomultiplier tubes (PMT) detector (R5509), the infrared luminescence signals through the emission monochromator (M300) were detected. The fluorescence decay curves were recorded with a NIR PMT (R5509) excited by a microsecond flash lamp (μF900). The visible up-conversion luminescence excited with a 30 mW diode laser at 980 nm was detected with a PMT detector (R928). All the measurements were carried out at room temperature.

3. Results and discussion

3.1. Partition of rare earth ions into nano-crystals

X-ray diffraction and transmission electron microscope analyses evidenced the amorphous structure of precursor glass and demonstrated the homogeneous distribution of spherical CaF_2 crystals with 15–25 nm in size among the glassy matrix after crystallization. As an example, TEM micrograph and corresponding SAED patter of 0.5 mol% Er^{3+}/0.5 mol% Yb^{3+} glass ceramic are presented in Fig. 1.

The near infrared emission spectra under 800 nm excitation recorded in the range of 900 to 1100 nm for the precursor glass and glass ceramics are presented in Fig. 2. The fluorescence spectra were detected under the same instrumental conditions for all the polished bulk samples with the same thickness of 3.0 mm. Compared with the precursor glass, the obvious augment of Er^{3+} emission intensities around 980 nm for the glass ceramics implies the incorporation of Er^{3+} ions into CaF_2 nano-crystals during crystallization, which decreased the non-radiative relaxation of Er^{3+} concentrated in lower phonon energy environment [11], and the occurring emission of Yb^{3+}in the range of 1020–1080 nm in co-doped glass ceramic, due to energy transfer from Er^{3+} to Yb^{3+} in nano-crystals, implies the

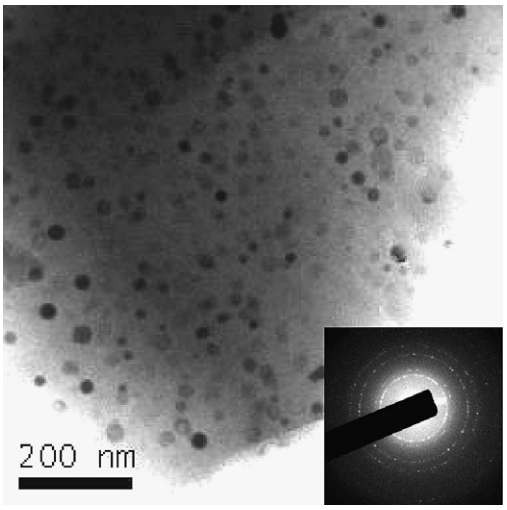

Fig. 1. TEM image and the corresponding selected area electron diffraction (SAED) pattern of 0.5 mol% Er^{3+}/0.5 mol% Yb^{3+} glass ceramic.

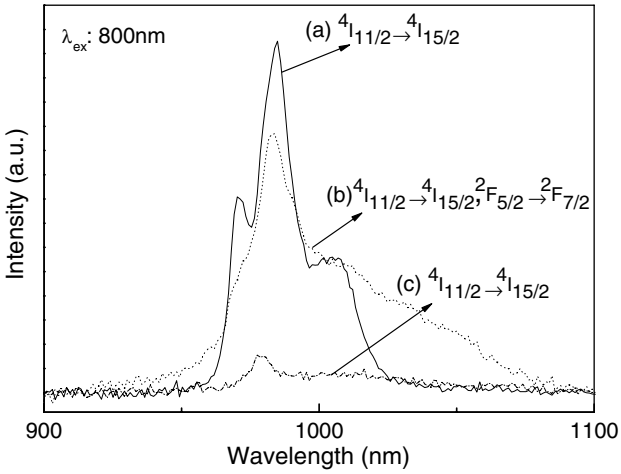

Fig. 2. The near infrared emissions under 800 nm excitation of: (a) 0.5 mol% Er^{3+}-doped glass ceramic, (b) 0.5 mol% Er^{3+}/0.5 mol% Yb^{3+} co-doped glass ceramic and (c) 0.5 mol% Er^{3+}/0.5 mol% Yb^{3+} co-doped glass.

partition of Yb^{3+} into nano-crystals too. The $^4I_{11/2} \rightarrow {}^4I_{15/2}$ fluorescence decays of Er^{3+} under 525 nm excitation measured at room temperature for 0.5 mol% Er^{3+}-doped precursor glass and glass ceramic are presented in Fig. 3. Therefore, the obvious increase of fluorescence lifetime from the precursor glass (97 μm) to the glass ceramic (616 μm) also supports the incorporation of Er^{3+} ions into CaF_2 nano-crystals. It is worthy to mention that the lifetime in glass ceramic is much low compared with the radiative lifetime in the bulk calculated by Judd–Ofelt theory [12], which could be ascribed to the following reasons: the enhanced non-radiative decay probability due to the short distance between Er^{3+} ions concentrated in CaF_2 nano-crystals; the integrated contribution of decay from Er^{3+} ions in CaF_2 nano-crystals and in glass matrix; and

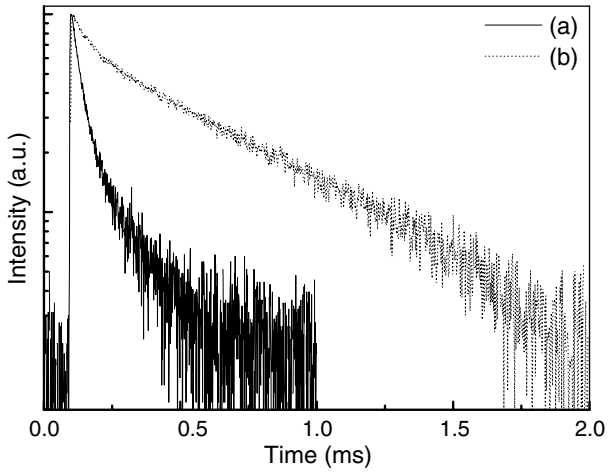

Fig. 3. Fluorescence decay curves from $^4I_{11/2}$ level of Er^{3+} under 525 nm excitation in: (a) 0.5 mol% Er^{3+}-doped glass and (b) glass ceramic.

the effect of nano-crystal size on the decay behavior of Er^{3+} incorporated in CaF_2.

In order to detect directly the distribution of rare earth ions in the sample, the energy dispersive X-ray spectroscopy (EDS) analysis with nano-sized probe on the glass matrix and an individual nano-crystal in 0.5 mol% Er^{3+}/0.5 mol% Yb^{3+} co-doped glass ceramic were conducted. The spectrum from the glass matrix, presented in Fig. 4a, shows high content of Si, Al, O and small amount of residual Ca and F, while Er and Yb contents are under detecting limit. As a comparison, the spectrum from an individual nano-crystal, shown in Fig. 4b, exhibits strong signals of Ca, F, Er and Yb (the Al, Si and O peaks are attributed to the matrix surrounding the nano-crystal), which further confirms that Er^{3+} and Yb^{3+} ions are mainly concentrated in CaF_2 crystals.

3.2. Fluorescence properties

The room temperature absorption spectra in the 350–1650 nm region of 0.5 mol% Er^{3+}-doped and 0.5 mol% Er^{3+}/1.0 mol% Yb^{3+} co-doped glass ceramic samples are shown in Fig. 5. The absorption bands are assigned to the transitions from the $^4I_{15/2}$ ground state to the excited states of Er^{3+} ions, and to the $^2F_{7/2} \rightarrow {}^2F_{5/2}$ transition of Yb^{3+} ions, respectively. In the co-doped sample the absorption bands in the range of 870–1100 nm correspond to the superposition of $^4I_{15/2} \rightarrow {}^4I_{11/2}$ transition of Er^{3+} plus $^2F_{7/2} \rightarrow {}^2F_{5/2}$ transition of Yb^{3+} ions. It is apparent that sensitization Yb^{3+} ions improve the excitation of Er^{3+}-doped glass ceramics, providing a broader and more intense absorption band suitable for laser diode excitation.

For Er^{3+} single-doped or Er^{3+}/Yb^{3+} co-doped precursor glasses, no up-conversion signals were detected. Fig. 6 shows the room temperature up-conversion fluorescence spectra of 0.5 mol% Er^{3+}-doped and 0.5 mol% Er^{3+}/

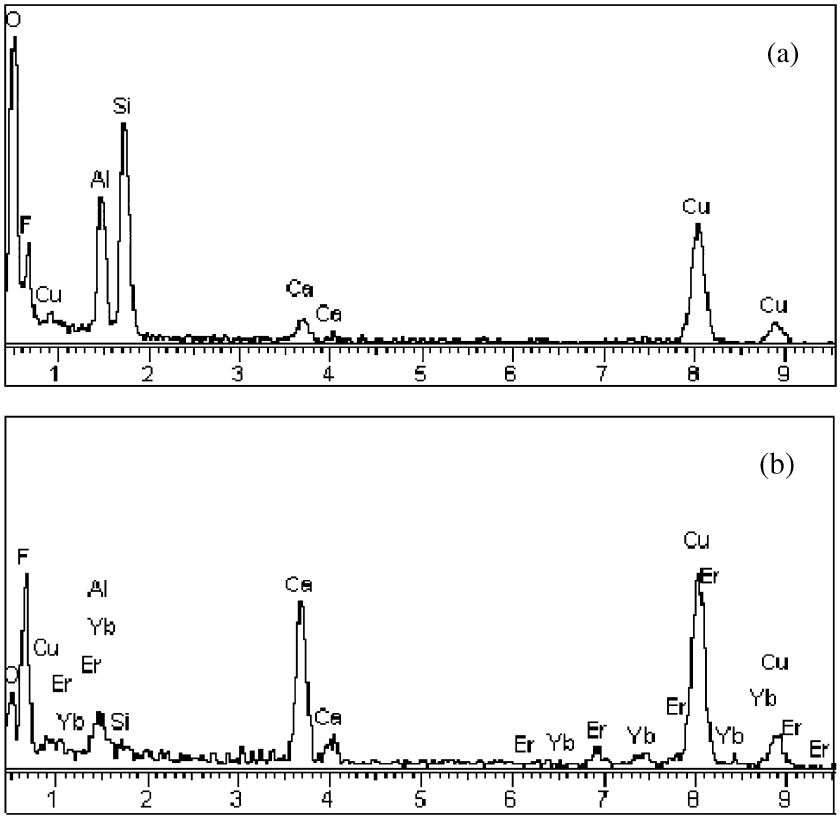

Fig. 4. EDS spectra from: (a) the glass matrix and (b) an individual CaF_2 nano-crystal in 0.5 mol% Er^{3+}/0.5 mol% Yb^{3+} co-doped glass ceramic; the presence of Cu peaks is due to copper grid used to support TEM specimen.

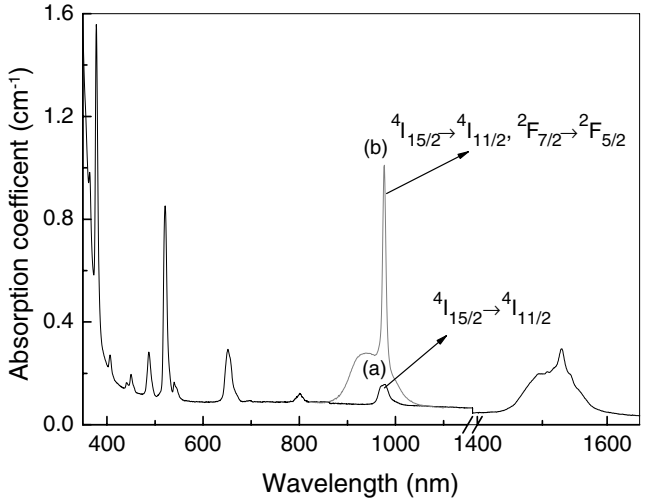

Fig. 5. Room temperature absorption spectra for: (a) 0.5 mol% Er^{3+}-doped and (b) 0.5 mol% Er^{3+}/1.0 mol% Yb^{3+} co-doped glass ceramics; the thickness of the samples is 3 mm.

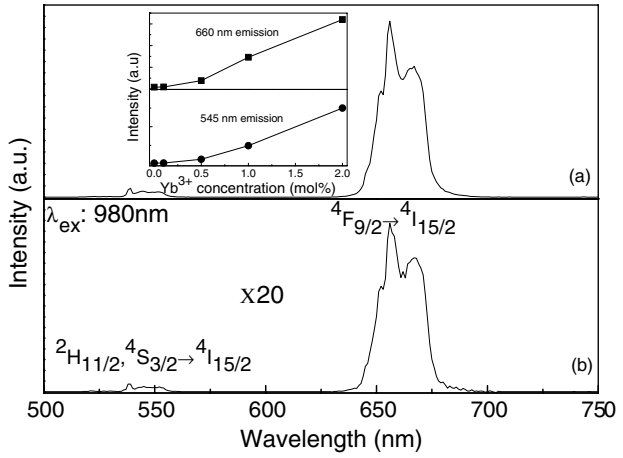

Fig. 6. Up-conversion fluorescence under 980 nm excitation for: (a) 0.5 mol% Er^{3+}/1.0 mol% Yb^{3+} co-doped and (b) 0.5 mol% Er^{3+}-doped glass ceramics; the inset shows the variation of up-conversion emission intensities under near-infrared excitation at 980 nm versus Yb^{3+} concentrations in the co-doped glass ceramics.

1.0 mol% Yb^{3+} co-doped glass ceramics under 980 excitation with the same instrumental conditions. For both samples, the up-conversion spectra show bands centered around 545 and 660 nm which are attributed to transitions of $^2H_{11/2}$, $^4S_{3/2} \rightarrow {}^4I_{15/2}$ and $^4F_{9/2} \rightarrow {}^4I_{15/2}$, respectively. It is found that the red emission is dominant in both samples, and the up-conversion emission intensities in co-doped sample is higher by a factor of about 20 than that in single-doped one, which confirms that there exists an effective energy transfer process between Yb^{3+} and Er^{3+} ions concentrated in CaF_2 nano-crystals. The inset of Fig. 6 shows the variation of up-conversion emission intensities of co-doped glass ceramics versus Yb^{3+} concentration. The intensities of green and red emissions strongly enhance, indicating the enhanced probability of energy transfer from Yb^{3+} to Er^{3+}, with increasing of Yb^{3+} concentration.

To investigate the excitation mechanisms for populating the $^2H_{11/2}$, $^4S_{3/2}$ and $^4F_{9/2}$ levels of Er^{3+} after infrared excitation, we measured the evolution of the up-conversion intensity for different pumping powers. In up-conversion processes the emission intensity I_{UP} is proportional to a power n of the infrared excitation intensity I_{IR}

$$I_{UP} \propto (I_{IR})^n \quad (1)$$

where n is the number of IR photons absorbed to populate per visible photon emitting. A plot of logarithm of I_{UP} versus logarithm of I_{IR} should yield a straight line with slope n. Fig. 7 shows such a plot for 0.5 mol% Er^{3+}/1.0 mol% Yb^{3+} co-doped glass ceramic, where the dependence of green or red emission intensity on the pump power is nearly quadratic (1.90 or 1.95 respectively), indicating two-photon up-conversion process to populate the $^2H_{11/2}$ and $^4S_{3/2}$ or $^4F_{9/2}$ levels. The same behavior is also performed in the single-doped [10] and other co-doped glass ceramics.

The fluorescence spectra around 1.53 μm of Er^{3+} single-doped precursor glass and co-doped glass ceramics with variation of Yb^{3+} concentration were recorded by exciting at 980 nm and shown in Fig. 8. All the samples were measured in the same conditions, enabling a comparison of the emission intensities. Compared with the emission of precursor glass, the appearance of Stark split peaks suggested the incorporation of Er^{3+} ions into CaF_2 nano-crystals in glass ceramics. The spectra of glass ceramic appear similar with fluorescence lines occurring at the same wavelength. The only difference is that the emission intensity enhances with increasing of Yb^{3+} concentration. The $^4I_{13/2} \rightarrow {}^4I_{15/2}$ fluorescence decays of Er^{3+} have been measured at room temperature for all the co-doped glass ceramics and presented in Fig. 9. With the increase of Yb^{3+} doping content, the electron population of Er^{3+} ions in $^4I_{13/2}$ level is largely

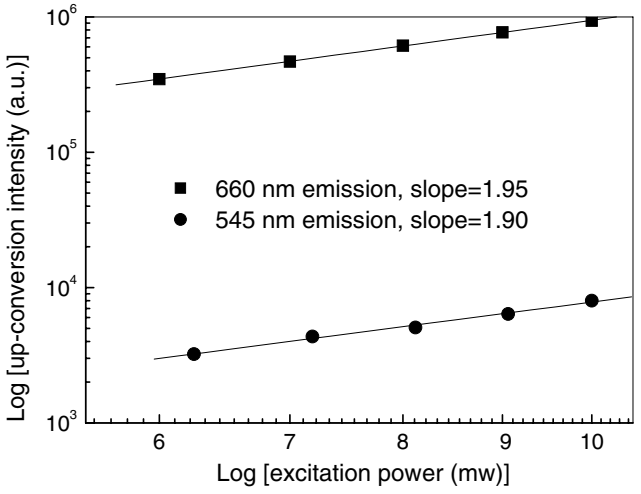

Fig. 7. Log–log plots of the up-conversion emission intensities as a function of the excitation power at 980 nm for 0.5 mol% Er^{3+}/1.0 mol% Yb^{3+} co-doped glass ceramic.

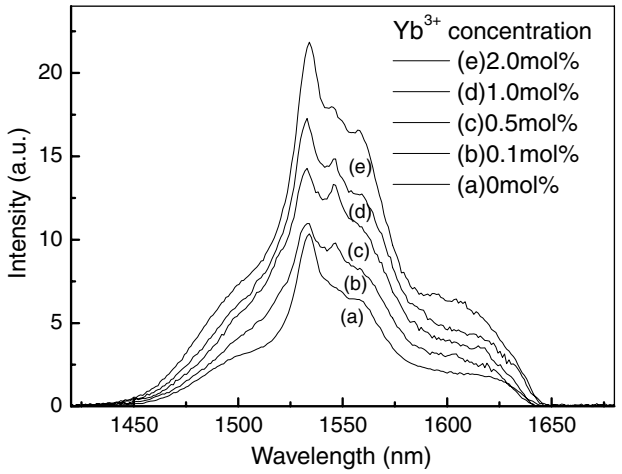

Fig. 8. Infrared fluorescence spectra of Er^{3+} single-doped precursor glass and Er^{3+}/Yb^{3+} co-doped glass ceramics under 980 nm excitation.

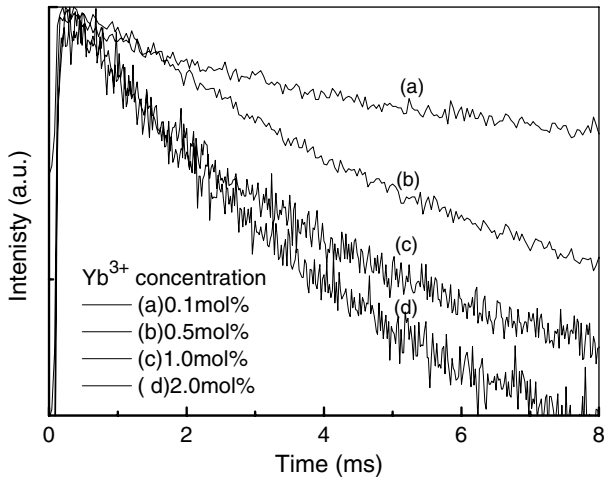

Fig. 9. Fluorescence decay curves from $^4I_{13/2}$ level of Er^{3+} under 980 nm excitation for all co-doped glass ceramics.

increased due to energy transfer from Yb^{3+} to Er^{3+}, which results in the enhancement of non-radiative decay probability of Er^{3+} and the decrease of lifetime of Er^{3+} $^4I_{13/2} \rightarrow {}^4I_{15/2}$ transition, as presented in Fig. 9.

3.3. Energy transfer and back transfer

In order to determine the $Yb^{3+} \rightarrow Er^{3+}$ energy transfer efficiency, the glass ceramics doped only with different content of Yb^{3+} were prepared, and their lifetimes were measured. For the Er^{3+}/Yb^{3+} co-doped samples, the energy transfer efficiency from Yb^{3+} to Er^{3+} can be evaluated by the following expression:

$$\eta = 1 - \tau_{Yb\text{–}Er}/\tau_{Yb} \quad (2)$$

where $\tau_{Yb\text{–}Er}$ and τ_{Yb} are $^2F_{5/2}$ lifetimes of Yb^{3+} ions with and without Er^{3+} ions, respectively. The inset of

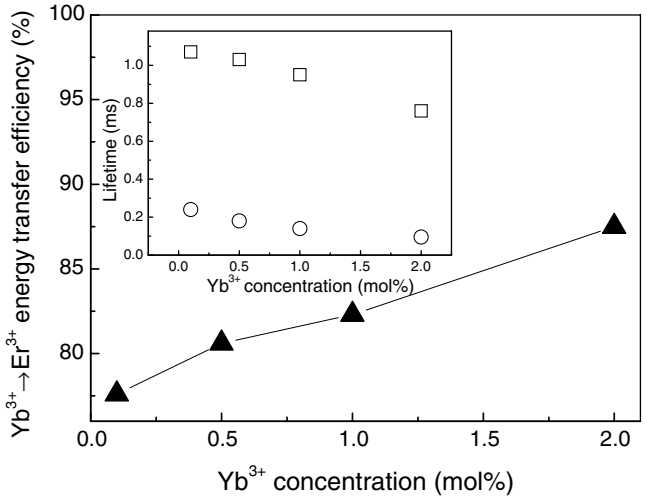

Fig. 10. $Yb^{3+} \rightarrow Er^{3+}$ energy transfer efficiency for the glass ceramics doped with different Yb^{3+} concentrations, the line is guide for the eyes; the inset shows the variation of Yb^{3+} lifetime as a function of Yb^{3+} concentration with (○) and without (□) Er^{3+} ions.

Fig. 10 presents the concentration dependence of the $^2F_{5/2}$ lifetime for the Er^{3+}/Yb^{3+} co-doped and the Yb^{3+} single-doped glass ceramics. The reasons for the lower lifetime of Yb^{3+} in single Yb^{3+}-doped glass ceramic than that in the bulk CaF_2 [13] is considered similar to those above discussion for Er^{3+} lifetime. The obvious decrease of Yb^{3+} lifetime from the Yb^{3+} single-doped sample to the co-doped one verifies the non-radiative characteristic of energy transfer from Yb^{3+} to Er^{3+}. The transfer efficiency as a function of donor concentration obtained from expression (2) is presented in Fig. 10. It is seen that the energy transfer efficiency increases with increasing of Yb^{3+} concentration, and excesses 85% for the sample of 0.5 mol% Er^{3+}/2.0 mol% Yb^{3+} co-doped glass ceramic. For the glass ceramics, Er^{3+} and Yb^{3+} ions are mainly incorporated into CaF_2 nano-crystals, and located closer to each other than those uniformly dispersed in the precursor glasses. The short distances between Er^{3+} and Yb^{3+} ions in CaF_2 nano-crystals favor inter-ionic interactions, resulting in an efficient energy transfer process.

In order to achieve better understanding on the energy transfer processes, the energy transfer and back transfer rates are quantitatively evaluated according to the rate equation formalism. These parameters are necessary for the further analyses of the performance of optical amplifiers as well as glass ceramic laser operations. Under continuous excitation with low pumping flux, the up-conversion excitation of Er^{3+} ions could not change appreciably the dynamics of $^4I_{11/2}$ level of Er^{3+} and $^2F_{5/2}$ level of Yb^{3+}, and thus will be neglected in the following analysis. The simplified energy level and energy transfer process between Er^{3+} and Yb^{3+} are given in Fig. 11. In the steady state rate equation formalism, the energy transfer processes can be described as follows:

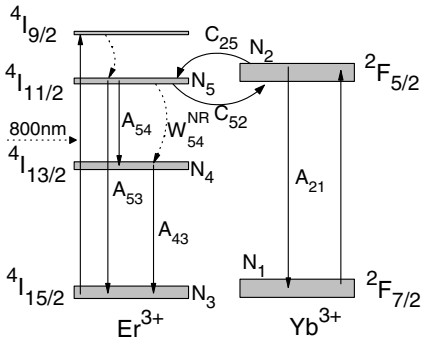

Fig. 11. Energy level scheme and transitions used to evaluate the transfer and back transfer rates in Er^{3+}/Yb^{3+} co-doped glass ceramics.

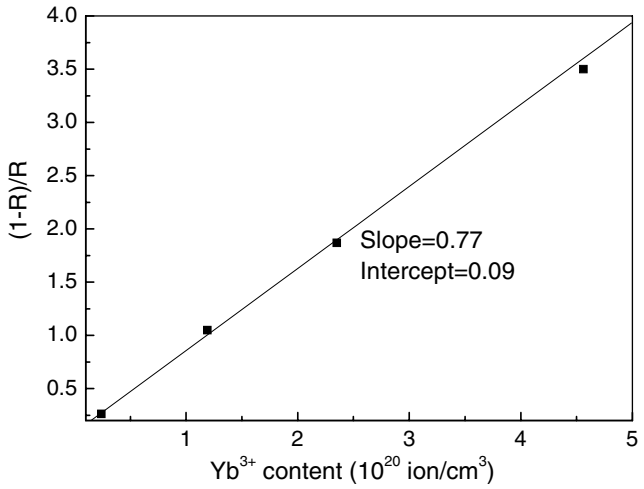

Fig. 12. The variation of $(1 - R)/R$ ratio versus Yb^{3+} concentration, the linear fitting results are also presented.

$$\frac{dN_2}{dt} = \sigma_{Yb}\Phi N_1 - (A_{21} + W_{21}^{NR})N_2 - C_{25}N_2N_3 + C_{52}N_5N_1 = 0 \quad (3)$$

$$\frac{dN_4}{dt} = (A_{54} + W_{54}^{NR})N_5 - (A_{43} + W_{43}^{NR})N_4 = 0 \quad (4)$$

$$\frac{dN_5}{dt} = C_{25}N_2N_3 - C_{52}N_5N_1 - (A_{54} + A_{53} + W_{54}^{NR})N_5 = 0 \quad (5)$$

where N_i is the population of the i-level, A_{ij} and W_{ij} the radiative and non-radiative transition probabilities between i and j states, σ_{Yb} the Yb^{3+} absorption cross-section at the pumping wavelength, Φ the pumping flux, and C_{25} and C_{52} the coefficients quantifying the energy transfer from Yb^{3+} to Er^{3+} and back transfer from Er^{3+} to Yb^{3+}, respectively. In addition, under the weak pumping condition, it is reasonable to assume that $N_1 \approx N_{Yb}$ and $N_3 \approx N_{Er}$.

Under 800 nm excitation, the erbium ions are excited to the $^4I_{9/2}$ multiplet. From the $^4I_{9/2}$ level, they relax non-radiatively to the $^4I_{11/2}$ multiplet. Then, either radiative and non-radiative intra-erbium relaxation or energy transfer to ytterbium ions can occur, so that the variation of the ratio (R) between the Er^{3+} emission ($^4I_{11/2} \rightarrow {}^4I_{15/2}$) and the total Er^{3+}/Yb^{3+} emission ($^4I_{11/2} \rightarrow {}^4I_{15/2}$ and $^2F_{5/2} \rightarrow {}^2F_{7/2}$) for different Er^{3+}/Yb^{3+} concentrations allows the determination of the transfer coefficients [14,15]

$$C_{52} = \frac{\beta}{\alpha}\tau_5^{-1} \quad (6)$$

$$C_{25} = \frac{A_{21}\tau_5^{-1}}{\alpha A_{53} N_{Er}} \quad (7)$$

where τ_5 is the measured lifetime of levels $^4I_{11/2}$, α and β are obtained by the least squares fitting of experimental data according to the following equation for glass ceramics doped with fixed Er^{3+} and various concentrations of Yb^{3+} (see Fig. 12):

$$\frac{1-R}{R} = \frac{A_{21}\tau_5^{-1}}{A_{53}C_{25}N_{Er}} + \frac{A_{21}C_{52}}{A_{53}C_{25}N_{Er}}N_{Yb} = \alpha + \beta N_{Yb} \quad (8)$$

The quantities of all the parameters in the last expression can be directly obtained from experimental measurements, and the transfer and back transfer coefficients are evaluated to be 5.8×10^{-16} and 1.3×10^{-16} cm^3/s, respectively, with $A_{21} = 438$ s^{-1} and $A_{53} = 111$ s^{-1}. The transfer coefficient is about 3.5 times higher than the back transfer one, being sufficient to provide high $^4I_{11/2}$ population of Er^{3+} to improve the fluorescence of the co-doped glass ceramics, as has been experimentally demonstrated stated above. It is worthy to mention that the derived transfer and back transfer coefficients are mainly originated from Er^{3+} and Yb^{3+} ions residing inside nano-crystals since there are almost no energy transfer detected in the precursor glasses.

4. Conclusions

Er^{3+}/Yb^{3+} co-doped transparent oxyfluoride glass ceramics containing CaF_2 nano-crystals were prepared with Er^{3+} and Yb^{3+} ions incorporated mostly into CaF_2. Compared with that of Er^{3+} single-doped glass ceramics, the emission intensities of 1.53 μm emission and infrared to visible up-conversion fluorescence of Er^{3+}/Yb^{3+} co-doped samples were significantly enhanced under 980 nm excitation due to energy transfer from Yb^{3+} to Er^{3+}. The quadratic pump power dependence of their green and red emission intensities indicates that these up-conversion transitions were ascribed to the two-photon absorption processes. The effective energy transfer efficiency, obtained from fluorescence decay lifetimes, increased with increasing of Yb^{3+} concentration. Using the rate equation formalism, the coefficients of energy transfer from Er^{3+} to Yb^{3+} and back transfer from Yb^{3+} to Er^{3+} for the investigated glass ceramic system were determined to be 5.8×10^{-16} and 1.3×10^{-16} cm^3/s, respectively.

Acknowledgment

This work was supported by the project of Nano-molecular Functional Materials of Fujian Province (2005HZ01-1), and the National Natural Science Foundation of China (Grant No. 50672098).

References

[1] B.D. Bartolo, Radiationless Processes, Plenum, New York, 1980.
[2] M. Mortier, F. Auzel, J. Non-Cryst. Solids 256&257 (1999) 361.
[3] A. Lucca, M. Jacquemet, F. Druon, F. Balembois, P. Georges, P. Camy, J.L. Doualan, R. Moncorgé, Opt. Lett. 29 (2004) 1879.
[4] Y. Wang, J. Ohwaki, Appl. Phys. Lett. 63 (1993) 3268.
[5] A.S. Gouveia-Neto, E.B. da Costa, L.A. Bueno, S.J.L. Ribeiro, J. Lumin. 110 (2004) 79.
[6] F. Lahoz, I.R. Martin, J. Mendez-Ramos, P. Núñez, J. Chem. Phys. 120 (2004) 6180.
[7] X. Qiao, X. Fan, M. Wang, Scripta Mater. 55 (2006) 211.
[8] P.A. Tick, Opt. Lett. 23 (1998) 1904.
[9] X. Qiao, X. Fan, J. Wang, M. Wang, J. Non-Cryst. Solids 351 (2005) 357.
[10] D.Q. Chen, Y.S. Wang, Y.L. Yu, E. Ma, Z.J. Hu, J. Phys: Condens. Mat. 17 (2005) 6545.
[11] T. Miyakawa, D.L. Dexter, Phys. Rev. B 1 (1970) 1961.
[12] G.A. Kumar, R. Riman, S.C. Chae, Y.N. Jang, I.K. Bae, H.S. Moon, J. Appl. Phys. 95 (2004) 3243.
[13] L. Su, J. Xu, H. Li, L. Wen, Y. Zhu, Z. Zhao, Y. Dong, G. Zhou, J. Si, Chem. Phys. Lett. 406 (2005) 254.
[14] B. Simondi-Teisseire, B. Viana, D. Vivien, A.M. Lejus, Opt. Mater. 6 (1996) 267.
[15] E. Cantelar, J.A. Muñoz, J.A. Sanz-García, F. Cussó, J. Phys: Condens. Mat. 10 (1998) 8893.